

OUTFLOWS NEAR AN ACCRETING BLACK HOLE: IONIZATION AND TEMPERATURE STRUCTURES

J. MARTIN LAMING¹ AND LEV TITARCHUK²

Received 2004 July 12; accepted 2004 October 4; published 2004 October 18

ABSTRACT

We calculate the temperature and ionization balance in an outflow from an accreting black hole under illumination by hard radiation from the central object. Electron scattering of the Fe K α photons within the highly ionized expanding flow leads to a decrease of their energy (redshift), which is of first order in v/c , when v is the outflow velocity and v is much less than the speed of light c . *This photon redshift is an intrinsic property of any outflow for which divergence is positive.* We also find that the equivalent widths of red-skewed Fe K α that originated in the wind is on the order of keV. We conclude that redshifted lines are intrinsic properties of the powerful outflows that are observed in many compact objects. Downscattering of the primary line photons generated in the outflow (a more natural and probable mechanism than the general relativistic effects in the innermost part of the accretion flow) leads to the formation of red-skewed lines.

Subject headings: accretion, accretion disks — atomic processes — black hole physics — galaxies: active — line: formation — radiation mechanisms: nonthermal

1. INTRODUCTION

There is a great need for a coherent physical picture predicting how X-ray spectra are produced near Galactic and extragalactic black hole (BH) sources. Elvis (2004) points out that the BH-disk-jet theory is presently a “high” theory, dealing only with overall energetics, and describes a naked object devoid of any of the veiling gas that presumably creates the observable spectral continuum and atomic features. This high theory fails to explain the various correlations between timing and spectral features observed in BH sources (for example, see details of these correlations in Mauche 2002; Titarchuk & Wood 2002; Titarchuk & Fiorito 2004). Elvis concludes that the community needs a “low” theory with sufficient detail to predict the emission (and presumably timing) and absorption phenomenology of BHs.

Many authors (e.g., Tanaka et al. 1995; Nandra et al. 1997; Wilms et al. 2001; Uttley et al. 2004; Miller et al. 2004) have found unusual curvature (red-skewed features) at energies between 2 and 8 keV in X-ray spectra of a number of Galactic and extragalactic BH sources. Significantly, the fluxes of these features remain nearly *constant* despite the large changes in the continuum flux from the central object as shown in the observations of MCG –6-30-15, NGC 4051, and others (Markowitz et al. 2003, hereafter MEV03), suggesting an origin in the outer regions of the accretion flow. In fact, MEV03 discuss the possibility of explaining the lack of correlation between the continuum and the line by using the ionized disk skin model of Nayakshin (2000) and Nayakshin & Kallman (2001; see also Ross et al. 1999). This model is consistent with the prediction that both broad and narrow K α lines should track continuum variations on timescales of months to years. However, such correlated behavior is not seen through the entire sample.

In this Letter, we further discuss a model for redshifting of emission lines by repeated electron scattering in a diverging outflow or wind. The basic mechanism is described by Titarchuk et al. (2003, hereafter TKB03). It is distinct from the proposals

for redshifts previously associated with outflows, Comptonization (in a low-temperature electron cloud; see Sunyaev & Titarchuk 1980, hereafter ST80, and Titarchuk & Shrader 2004 for details), and the general accelerating outflow model of Sobolev (1957), both of which were correctly ruled out by Fabian et al. (1995) in connection with the redshifted Fe K α in MCG –6-30-15. Fabian et al. argue that the major problem with this outflow model is that MCG –6-30-15 has a warm absorber. The O VII edge in the absorber indicates that the flow along the line of sight is less than about 5000 km s^{–1} (Fabian et al. 1994), which seriously conflicts with outflow of about 100,000 km s^{–1} required by the accelerating outflow model. Laurent & Titarchuk (2004, hereafter LT04) confirm that the velocity of the warm absorber outflow in MCG –6-30-1 is about 5000 km s^{–1} using Monte Carlo simulations of the K α line propagation in the constant-velocity wind. They present the results of fitting the wind model to the *XMM* (EPIC) data of Wilms et al. (2001) obtained during the observation of MCG –6-30-15. These observations were focused on the broad Fe K α line at ~6.4 keV. The continuum has been fitted with a power law of index 1.8, and the residuals have been fitted using the wind model. The best-fit model parameters they found are $E_{\text{ph}} = 6.5$ keV, $kT = 0.1$ keV, $\tau_{\text{T}} = 1.7$, and $\beta = v/c = 0.02$, where $E_{\text{ph}} = h\nu_{\text{ph}}$ is the energy of the primary K α photons and kT is the temperature of the wind, respectively. Downscattering of the primary line photons in the outflow leads to the formation of red-skewed lines. This effect is seen even when the outflow optical depth τ_{T} is about 1–2 and $\beta = v/c \approx 0.02$.

A thorough analysis and review of the diffusion theory of photon propagation in an optically thick fluid in a bulk outflow has been provided by TKB03. They show that the iron line is produced in an effectively optically thick medium. Its red wing is the result of multiple scattering, each scattering producing a first-order v/c redshift (see Fig. 1 for a simple explanation of the outflow redshift effect). The TKB03 results are obtained using the Fokker-Planck equation (Blandford & Payne 1981), which is valid for $\beta = v/c \ll 1$ and $\tau_{\text{T}} > 1$. The Monte Carlo method does not have these limitations in terms of β and τ_{T} . Using a Monte Carlo method, LT04 have made extensive radiative transfer simulations in a bulk outflow from a compact object (black hole or neutron star). They find that electron scattering of the photon within the expanding flow leads to a decrease of its

¹ Naval Research Laboratory, Space Science Division, Code 7674L, 4555 Overlook Avenue, SW, Washington, DC 20375-5352; jlaming@ssd5.nrl.navy.mil.

² Center for Earth Observing and Space Research, George Mason University, Fairfax, VA 22030; and Naval Research Laboratory, Space Science Division, Code 7655, 4555 Overlook Avenue, SW, Washington, DC 20375-5352; ltitarchuk@ssd5.nrl.navy.mil.

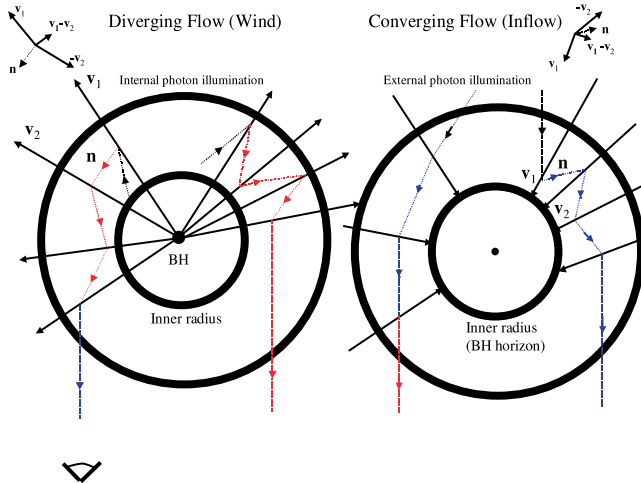


FIG. 1.—*Left:* Schematic diagram showing wind geometry. The outflow (wind) originates at the inner radius. The radii of the optical depth in the Fe K continuum and the electron scattering optical depth are of order unity. A photon emitted near the inner boundary and subsequently scattered by an electron moving with velocity \mathbf{v}_1 is received by an electron moving with velocity \mathbf{v}_2 as shown. The change in frequency is $\nu_2 = \nu_1[1 + (\mathbf{v}_1 - \mathbf{v}_2) \cdot \mathbf{n}/c]$, where \mathbf{n} is a unit vector along the path of the scattered photon at the scattering point. In a diverging flow, $(\mathbf{v}_1 - \mathbf{v}_2) \cdot \mathbf{n}/c < 0$ and photons are successively redshifted until they are scattered to an observer at infinity. The color of the photon path indicates the frequency shift in the rest frame of the receiver (electron or the Earth observer). *Right:* In a converging flow, $(\mathbf{v}_1 - \mathbf{v}_2) \cdot \mathbf{n}/c > 0$ and photons are blueshifted.

energy, which is of first order in v/c . LT04 demonstrate that the emergent line iron profile exhibits a broad redshifted feature. They also find so-called negative time lags, related to the time dependence of the photon energy losses from propagating out of the flow. In this Letter, we argue that the Fe K α line is naturally produced in an external outflow illuminated by the hard X-radiation coming from the central source (BH) and the red-skewed features are the result of scattering of iron line photons in the outflow. We offer a model in which the hard radiation of the central object illuminates and heats the outflow region that originated in the outskirts of the disk (well outside the innermost part of the accretion disk near the BH). We present details of self-consistent calculations of atomic features and temperature structure within the outflow. The result of these calculations for $\beta = 0$ gives us the temperature and ionization structure within the disk.

In § 2, we present a description of the outflow illumination model and provide the main idea of the photon frequency shift due to electron scattering in the diverging flow (outflow) and converging flow (inflow). In § 3, we show the results of calculations of temperature and ionization balance in the outflow and evaluation of the equivalent widths of Fe K α as a function of the ionization parameter for various incident X-ray spectral distributions and outflow bulk velocity β . Discussion and conclusions follow in § 4.

2. OUTFLOW ILLUMINATION BY BLACK HOLE X-RADIATION: EFFECT OF THE K α PHOTON OUTFLOW REDSHIFT AND SUPPRESSION OF THE BLUE WING OF THE K α LINE

Our basic scenario is illustrated in Figure 1. The wind originates at a distance R_{inner} from the central black hole and is of a density such as to give a Thomson scattering optical depth τ_T close to unity far from the black hole. The optical depth in the Fe K continuum is about 1–3 times higher than that due to

electron scattering (assuming a solar abundance of Fe and depending on charge state; see Kallman et al. 2004), and so Fe K α formed by inner shell ionization of Fe ions in the outflow by the continuum from the central black hole only comes from a smaller inner region. So long as $R(\tau_{\text{Fe K}} \sim 1) < R(\tau_T \sim 1)$, the Fe K α equivalent width is insensitive to the Fe abundance assumed. A lower Fe abundance increases $R(\tau_{\text{Fe K}} \sim 1)$, and consequently Fe K α forms over a larger volume. This figure also illustrates the redshift of photons in the diverging flow. A photon emitted near the inner boundary and subsequently scattered by an electron moving with velocity \mathbf{v}_1 is received by an electron moving with velocity \mathbf{v}_2 as shown with frequency $\nu_2 = \nu_1[1 + (\mathbf{v}_1 - \mathbf{v}_2) \cdot \mathbf{n}/c]$, where \mathbf{n} is a unit vector along the path of the photon at the scattering point. In a diverging flow, $(\mathbf{v}_1 - \mathbf{v}_2) \cdot \mathbf{n}/c < 0$ and photons are successively redshifted, until scattered to an observer at infinity. In a converging flow, $(\mathbf{v}_1 - \mathbf{v}_2) \cdot \mathbf{n}/c > 0$ and photons are blueshifted. Any photon with energy of about 7–8 keV and higher interacting with outflow plasma is more likely to be absorbed by the flow and be reemitted at energies of about 6.4–6.6 keV (depending on the ionization stage of the flow) instead of being scattered by electrons there. This photoabsorption effect is particularly important in the view of the main claim of this work, which is that it suppresses the blue wing at the expense of the K α emission at energies of about 6.4–6.6 keV.

3. TEMPERATURE AND IONIZATION BALANCE IN THE OUTFLOW

Formulation of the problem.—The temperature and ionization balance in the outflow is determined by seeking the temperature at which the outflowing gas attains photoionization-recombination equilibrium. The gas is heated by Compton scattering and photoionizations by photons from the central compact object and is cooled by radiation, ionization, and adiabatic expansion losses. We take collisional ionization and recombination rates from Mazzotta et al. (1998), photoionization cross sections from Verner et al. (1996), and radiative power losses from Summers & McWhirter (1979). For the Fe K photoionizations, we modify the Verner et al. (1996) cross sections by a multiplicative factor in the range 1–3 depending on charge state to bring these cross sections into better agreement with the more recent work of Kallman et al. (2004). It is evident that the temperature and ionization structure in the disk due to illumination of the hard radiation can be obtained as a result of this solution for $\beta = v/c = 0$.

Results of calculations.—For each inner wind radius, we define a density that gives an electron scattering opacity in the wind τ_T , thus density $n \propto \tau_T/R_{\text{inner}}$, where R_{inner} is the inner radius of the wind. In outer portions of the wind, the density varies as $n \propto 1/R^2$, so the ionization parameter, L/nR^2 , remains approximately constant. The Compton and photoelectric heating rates, approximately proportional to $n/R^2 \propto 1/R^4$, fall off slightly faster than the cooling rate (proportional to $n/R \propto 1/R^3$ for adiabatic expansion, proportional to $n^2 \propto 1/R^4$ for radiative losses) in a realistic wind. The temperature we calculate at the inner edge of the wind is the highest temperature in the flow in cases where adiabatic expansion dominates the cooling. Where radiative cooling is more important, the heating and cooling are more evenly balanced, and the temperature we calculate is likely to be approximately correct throughout the flow. Detailed radiation transfer modeling accounting for successive absorption and scattering of the incident hard spectrum to improve upon this estimate is beyond the scope of this work.

In Figure 2, we plot the run of plasma temperature against

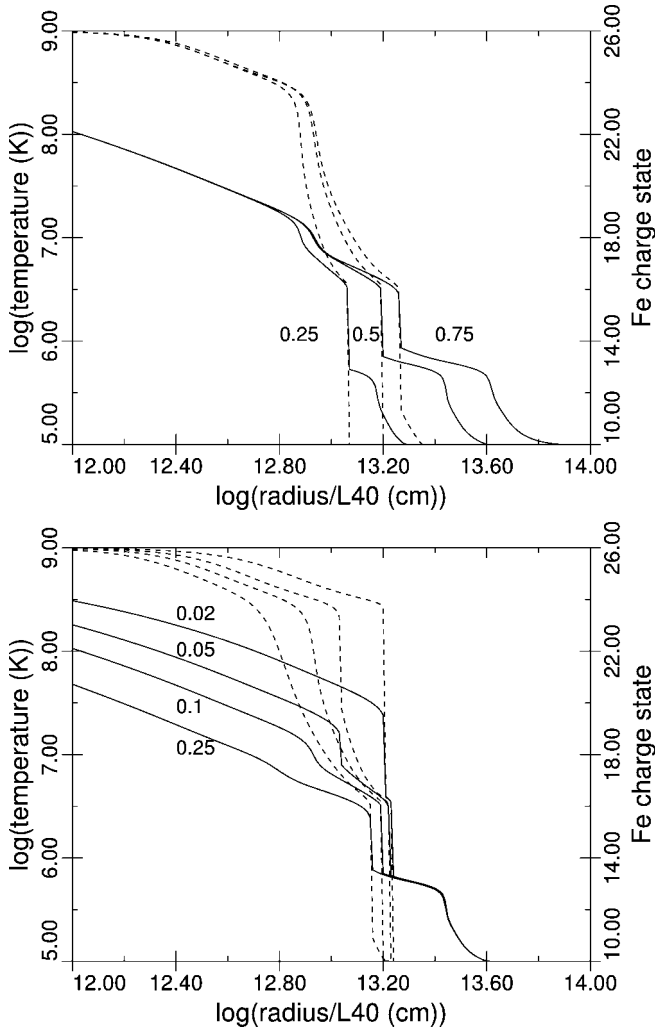


FIG. 2.—Plot of temperature at R_{inner} against R_{inner} for an accretion wind (solid lines). The inner radius R_{inner} scales with the central source luminosity and the optical depth of the wind shell τ_T . For any $\tau_T \neq 1$, the temperature is a function of $\tau_T R_{\text{inner}}/L_{40}$. The top panel shows results for expansion speed $\beta = v/c = 0.1$ and spectral indices $\alpha = 0.25, 0.5$, and 0.75 . The bottom panel shows the results for $\alpha = 0.5$ and $\beta = v/c = 0.02, 0.05, 0.1$, and 0.25 . The dashed lines show the average Fe charge state (to be read on the right-hand axis).

initial wind radius for a variety of models. The top panel shows temperature (solid line; to be read on the left-hand y-axis) and average Fe charge state (dashed line; to be read on the right-hand y-axis) for an outflow with $\beta = v/c = 0.1$ and for incident spectra $I(\nu) \propto \nu^{-\alpha} \exp(-h\nu/2kT)$ with $\alpha = 0.25, 0.5$, and 0.75 and $kT = 50$ keV. The inverse of the ionization parameter $nR^2/L \approx \tau_T R_{\text{inner}}/L_{40}$ on this plot, where L_{40} is the source luminosity in units of 10^{40} ergs s $^{-1}$. For $\tau_T R_{\text{inner}}/L_{40} < 10^{12.8}$ cm, Fe is in the He-like charge state or higher, and adiabatic expansion dominates the cooling. As L shell ions Fe XVII–XXIV start to form, radiative cooling begins to dominate and the temperature drops more steeply, with regions of thermal instability between Fe charge states +16 and +13. Harder spectra (i.e., lower α) with more photons at high energies have slightly lower photoionization rates for charge states Fe $^{+23}$ and below (for the same luminosity), and so under these conditions the outflowing plasma recombines and cools slightly faster. The bottom panel shows similar plots but now with $\alpha = 0.5$ and $\beta = v/c = 0.02, 0.05, 0.1$, and 0.25 . Faster outflows give more adiabatic cooling and so cool and recombine at lower radii than do the lower outflows.

Figure 3 shows the equivalent widths of Fe K α (dashed lines;

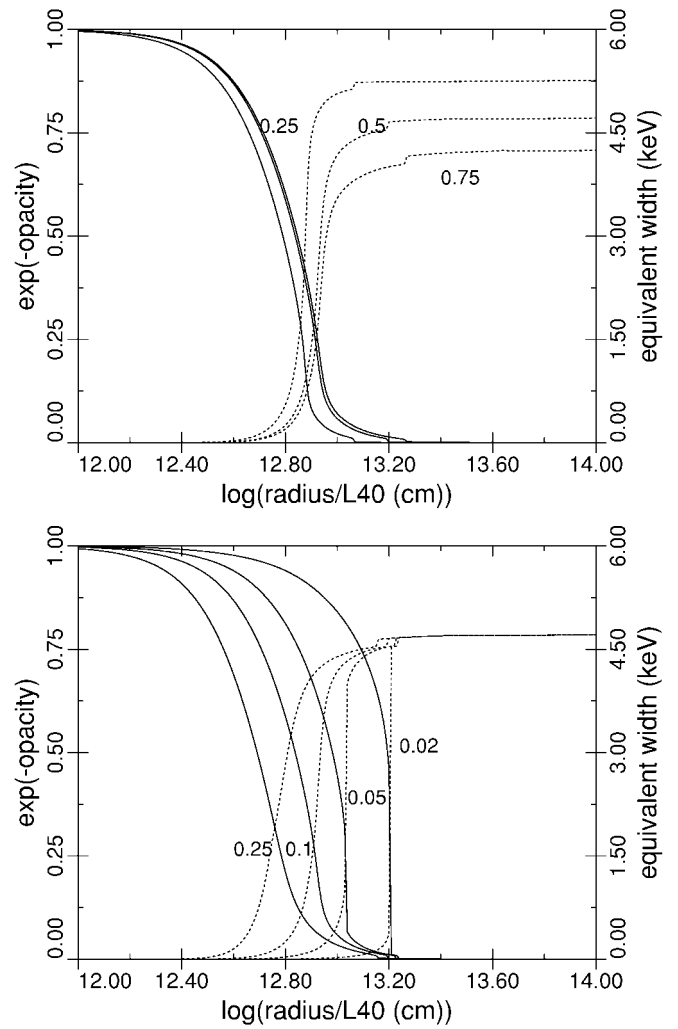


FIG. 3.—Plots of the equivalent width of Fe K α (dashed lines) produced by inner shell ionization of Fe in an accretion wind by continuum from the central source, for the same parameters as in Fig. 2. At small radii, the equivalent width is essentially zero because Fe is in charge state 24 or higher, with no L shell electrons available to fill a K shell vacancy. As Fe recombines at larger radii, the equivalent width increases. The solid lines to be read on the left-hand axis give the total opacity in the outflow at 4 keV, in the form $\exp(-\text{opacity})$. The predicted equivalent width at large radii of about 5 keV is significantly larger than that observed of about 1 keV. However, the total wind opacity at these radii is such that most of the Fe K line would be absorbed further out. Only for $\tau_T R_{\text{inner}}/L_{40}$ out to where the equivalent width is approximately 1 keV is the opacity sufficiently small to allow the line to be observed.

to be read on the right-hand axis) for the same sets of parameters as for Figure 2. The solid lines to be read on the left-hand axis give the total opacity in the outflow at 4 keV, in the form $\exp(-\text{opacity})$. At small radii, the equivalent width is essentially zero because Fe is in charge state 24 or higher, with no L shell electrons available to fill a K shell vacancy. As Fe recombines at larger radii, the equivalent width increases. The predicted equivalent width at large inner radii of about 5 keV is significantly larger than that observed of about 1 keV. However, the total wind opacity at these radii is such that most of the Fe K line would be absorbed further out. Only for $R_{\text{inner}} \sim 10^{13} L_{40}/\tau_T$ and consequently for the wind temperatures about a few times 10^6 K (see Figs. 2 and 3) to where the equivalent width is approximately 1 keV is the opacity sufficiently small to allow the line to be observed. We also note that this opacity is likely to have the effect of suppressing any Fe L shell features between 1 and 2 keV photon energy.

4. DISCUSSION AND CONCLUSIONS

We find the self-consistent temperature and ionization structure of the wind shell as a function of the parameter (radius/luminosity, $\tau_T R_{\text{inner}}/L_{40}$, where R_{inner} is the inner outflow radius and L_{40} is X-ray luminosity in units of 10^{40} ergs s^{-1}) for a given shell Thomson optical depth τ_T . It is evident that the ionization parameter L_{40}/nR^2 is constant through the shell (i.e., for $R > R_{\text{inner}}$) if the velocity of the wind is constant through the flow. The constraints on the Fe ionization balance and the opacity in the wind dictate a possible range of interest of $\tau_T R_{\text{inner}}/L_{40}$ values around 10^{13} cm. Thus, our solution allows us to determine the size of the shell base for a given luminosity for which the red-skewed line is observed. For typical low/hard-state luminosities of a few times 10^{36} – 10^{37} ergs s^{-1} , when the red-skewed line is really observed in galactic black holes the inner radius of the shell is a few times 10^9 – 10^{10} cm for the optical depth of the wind of order unity. It means that the inner radius of the wind shell is about 10^3 – 10^4 Schwarzschild radii. One can obtain the similar size of the wind shell in Schwarzschild radii units for extragalactic sources because the luminosity and the Schwarzschild radius is linearly scaled with BH mass.

It is important to note that if the Thomson optical depth of outflow is of order of unity, then the mass outflow rate \dot{M}_{out} is of order of the Eddington mass accretion rate \dot{M}_{Edd} and higher (see, e.g., eq. [4] in King & Pounds 2003, hereafter KP03). King (2004) and KP03 present strong arguments that powerful mass outflows from Eddington-limited accreting compact objects appear to be a very widespread phenomenon. They further argue that they may provide the soft excess observed in quasars and ultraluminous X-ray sources and imply that such objects have a major effect on their surroundings. Recent *XMM-Newton* observations of bright quasars (Pounds et al. 2003a, 2003b; Reeves et al. 2003) give strong evidence for powerful outflows from the nucleus with mass rates $\dot{M}_{\text{out}} \sim \dot{M}_{\odot} \text{ yr}^{-1} \sim \dot{M}_{\text{Edd}}$ and velocity $v \sim 0.1c$ (i.e., $\beta = 0.1$) in the form of blueshifted X-ray absorption lines. These outflows closely resemble those recently inferred from a set of ultraluminous X-ray sources with extremely soft spectral components (Mukai et al. 2003; Fabbiano et al. 2003). Furthermore, if the outflow optical depth is really about 1 in the low/hard state (when the X-ray luminosity is much less than the Eddington luminosity), one can conclude that in the

low/hard state the disk mass accretion rate is only a very small fraction of the outflow mass rate. In fact, this ratio of the accretion and outflow rates was predicted by Blandford & Begelman (1999), who developed the pure hydrodynamical model (the “ADIOS” model). The main point of the ADIOS model is that only a tiny fraction of the gas supplied actually falls onto the black hole. This is precisely what we obtain using the diverging flow model.

We conclude that the range of the parameter $\tau_T R_{\text{inner}}/L_{40}$ (proportional to the inverse of the so-called ionization parameter used in the literature) is about 10^{13} when the observed $K\alpha$ lines of the ~ 1 keV equivalent widths are presumably produced in the wind. The wind temperature (in such a case) is about a few times 10^6 K. Thus, our study shows that the strong iron line with its red-skewed feature can be generated in the relatively cold extended region far away from the source of the illuminating photons (of order 10^3 – 10^4 Schwarzschild radii).

On the other hand, one can argue that the “standard” cold disk plus hot corona explanation for the broad lines is “very robust (it needs only the cold disk and a hot corona),” and one does not need any other explanation for this effect. In fact, the so-called cold disk can survive under the hot corona only if the corona is situated at least $(10^3 - 10^4)/\tau_T$ Schwarzschild radii away, where τ_T is the Thomson optical depth of the disk. If the corona is much closer, the disk as a target illuminated by the hard radiation of the corona is very hot and finally evaporates. It is evident from Figs. 2 and 3 that the temperature goes to 10^9 K and the $K\alpha$ equivalent width goes to zero as $\tau_T R_{\text{inner}}/L_{40} \ll 10^{13}$ cm for $\beta < 0.05$. Other points regarding the “robustness” of the standard interpretation are: Even if the line is produced in the disk, how one can see $K\alpha$ through the corona if the corona optical depth τ_{cor} is of order of 1 and the corona electron temperature is about 50–60 keV? The directed radiation of the $K\alpha$ emission is attenuated exponentially as $\exp(-\tau_{\text{cor}}/\mu)$ (at least) $< \frac{1}{3}$, where μ is the cosine of the inclination angle. But the scattered component is completely smeared out—the relative energy change of the line photon at any scattering is $\langle \Delta E/E \rangle = 4kT/m_e c^2 = 0.5$ (see, e.g., ST80).

J. M. L. is supported by basic research funds of the Office of Naval Research. L. T. is supported by the George Mason University Center for Earth Observing and Space Research.

REFERENCES

- Blandford, R. D., & Begelman, M. C. 1999, MNRAS, 303, L1
 Blandford, R. D., & Payne, D. G. 1981, MNRAS, 194, 1033
 Elvis, M. 2004, in ASP Conf. Ser. 311, AGN Physics with the Sloan Digital Sky Survey, ed. G. T. Richards & P. B. Hall (San Francisco: ASP), 109
 Fabbiano, G., King, A. R., Zezas, A., Ponman, T. J., Roots, A., & Schweizer, F. 2003, ApJ, 591, 843
 Fabian, A. C., et al. 1994, PASJ, 46, L59
 ———. 1995, MNRAS, 277, L11
 Kallman, T. R., Palmeri, P., Bautista, M. A., Mendoza, C., & Krolik, J. H. 2004, ApJS, submitted (astro-ph/0405210)
 King, A. R. 2004, Nucl. Phys. B, 132, 376
 King, A. R., & Pounds, K. A. 2003, MNRAS, 345, 657 (KP03)
 Laurent, P., & Titarchuk, L. 2004, ApJL, submitted (LT04)
 Markowitz, A., Edelson, R., & Vaughan, S. 2003, ApJ, 598, 935 (MEV03)
 Mauche, C. W. 2002, ApJ, 580, 423
 Mazzotta, P., Mazzitelli, G., Colafrancesco, S., & Vittorio, N. 1998, A&AS, 133, 403
 Miller, J., et al. 2004, ApJ, 601, 450
 Mukai, K., Pence, W. D., Snowden, S. L., & Kuntz, K. D. 2003, ApJ, 582, 184
 Nandra, K., George, I. M., Mushotzky, R. F., Turner, T. J., & Yaqoob, T. 1997, ApJ, 477, 602
 Nayakshin, S. 2000, ApJ, 540, L37
 Nayakshin, S., & Kallman, T. 2001, ApJ, 546, 406
 Pounds, K. A., King, A. R., Page, K. L., & O’Brien, P. T. 2003a, MNRAS, 346, 1025
 Pounds, K. A., Reeves, J. N., King, A. R., Page, K. L., O’Brien, P. T., & Turner, M. J. L. 2003b, MNRAS, 345, 705
 Reeves, J. N., O’Brien, P. T., & Ward, M. J. 2003, ApJ, 593, L65
 Ross, R., Fabian, A. C., & Young, A. 1999, MNRAS, 306, 461
 Sobolev, V. V. 1957, Soviet Astron., 1, 678
 Summers, H. P., & McWhirter, R. W. P. 1979, J. Phys. B, 12, 2387
 Sunyaev, R. A., & Titarchuk, L. G. 1980, A&A, 86, 121 (ST80)
 Tanaka, Y., et al. 1995, Nature, 375, 659
 Titarchuk, L., & Fiorito, R. 2004, ApJ, 612, 988
 Titarchuk, L., Kazanas, D., & Becker, P. A. 2003, ApJ, 598, 411 (TKB03)
 Titarchuk, L., & Shrader, C. 2004, ApJ, in press (astro-ph/0408261)
 Titarchuk, L., & Wood, P. A. 2002, ApJ, 577, L23
 Uttley, P., Taylor, R. D., McHardy, I. M., Page, M. J., Mason, K. O., Lamer, G., & Fruscione, A. 2004, MNRAS, 347, 1345
 Verner, D. A., Ferland, G. J., Korista, K. T., & Yakovlev, D. G. 1996, ApJ, 465, 487
 Wilms, J., et al. 2001, MNRAS, 328, L27